Vortex stabilization in Bose-Einstein condensate of alkali-metal atom gas

Tomoya Isoshima* and Kazushige Machida

Department of Physics, Okayama University, Okayama 700-8530, Japan

(Received 15 July 1998)

A quantized vortex in Bose-Einstein condensation (BEC) of an alkali-metal atom gas is known to be unstable intrinsically at zero temperature. We examine two stabilization mechanisms of a vortex theoretically. (i) The finite temperature effect is shown to stabilize a vortex. (ii) An additional pinning potential, which may be produced by a focused laser beam at the vortex center, is also shown to stabilize it even at zero temperature. The mean-field calculation for BEC confined by a harmonic potential is employed. The detailed properties of a stable vortex are given, such as the spatial profiles of the condensate and noncondensate, the particle current density around the core, the whole excitation spectrum, and their temperature dependence. [S1050-2947(99)01503-6]

PACS number(s): 03.75.Fi, 05.30.Jp, 67.40.Vs

I. INTRODUCTION

Many-body dilute Bose systems have been the focus in condensed-matter physics since the experimental realization of Bose-Einstein condensation (BEC) in alkali-metal atom gases at ultralow temperatures [1–3]. There are many recent theoretical and experimental works devoted to the elucidation of BEC [4,5]. Experimental works are mainly conducted for dilute Bose systems, whose atom number is typically $\sim O(10^6)$ for ^{23}Na and ^{87}Rb. Gases are confined magnetically in a harmonic trap. The BEC transition temperatures are in a range of $O(\mu K)$. The experimental forefront is rapidly extending; one can tune the particle-particle interaction constant by utilizing the so-called Feshbach resonance phenomena [6] or one can confine a system purely optically so that several atomic hyperfine substates are simultaneously condensed, giving rise to an opportunity to explore BEC with internal degrees of freedom [7–9]. Several proposals of experimental methods to realize a vortex state have been made theoretically [5,10,11]. This paper concerns the vortex states in a somewhat different way.

As for the earlier theoretical developments, the microscopic theoretical work on BEC started with Bogoliubov [12] long ago and has been followed by important progress, such as by Gross [13], Pitaevskii [14], Iordanskii [15], Fetter [16], and Popov [17]. These mean-field theories are particularly suited for treating the present gaseous BEC systems trapped optically or magnetically in a restricted geometry. Therefore, the current theoretical studies [18] mainly focus on examining these mean-field theories to extract the spatial structures of the condensate and noncondensate and low-lying collective modes. The agreement between these mean-field theories and experiments is fairly good [5].

Previously we have demonstrated that the Bogoliubov approximation of the mean-field theory cannot sustain a stable vortex [19]. This somewhat unexpected result, which had been suggested by Dodd *et al.* [20], is now clearly explained

physically by Rokhsar [21], who shows that the vortex is always unstable against the translational mode with zero energy. Thus the vortex core in a cylindrically symmetric harmonic trap spirals out towards the outside of a system where the condensate density is low.

The main purpose of this paper is to examine the stability of a quantized vortex, which is directly related to the question of superfluidity of the present BEC systems. This instability can be expressed numerically either by comparing the free energy of systems with and without a vortex (stability) or by checking whether or not an eigenstate with a negative eigenvalue exists in a system with vortices (metastability). The latter is far more serious than the former and is discussed in this paper as ''stability.''

In the present paper, which follows our previous papers [19,22] based on the same formalism and numerical procedure, we show that the intrinsic instability of a quantized vortex can be remedied either by raising the temperature T or by introducing the pinning potential at the center of a cylindrically symmetric rectilinear vortex line, which prevents the vortex from spiraling out. The latter method for the vortex stabilization has been pointed out by several authors [5], whose experimental feasibility seems to be quite high since it may be easy to realize a desired pinning potential by sending a focused laser beam to the vortex center. Here we provide microscopic self-consistent calculations within the Popov approximation (PA), yielding detailed properties of a stable vortex, beyond Gross-Pitaevskii theory which treats only the condensate component. This enables us to discuss the vortex at finite temperatures. A comparative study of various approximations, including the PA, is presented in Ref. [19]. The PA is a gapless approximation and is believed to be reliable at low temperatures. As for the improvement of the Popov approximation, Hutchinson *et al.* proposed a theory [23].

Various spatial structures of the quantized vortex in rotating BEC systems are investigated based on this scheme of stabilization. This investigation is important since the microscopic understanding of the vortex based on the self-consistent picture has been lacking so far, except for a few attempts [24–26] for present BEC systems. Several points

---

*Electronic address: tomoya@mp.okayama-u.ac.jp

are worth exploiting: (i) the spatial profiles of the condensate and noncondensate, (ii) the dispersion relation of the excitation spectrum of the system, and (iii) the low-lying excitations localized around a vortex core, which is known as the Kelvin mode [27]. These features may be directly observable and should be compared with those in vortices in a superconductor where extensive studies have been compiled [28].

The arrangement of this paper is as follows. In Sec. II we recapitulate the Popov approximation, which is one of the various types of mean-field theories (see, for example, Refs. [19,29]) due originally to Bogoliubov [12]. We explain our numerical procedure to solve a self-consistent equation within the PA. In Sec. III the physical origin of stabilization is discussed and the detailed calculations for a stable vortex at finite temperatures are shown. We also compare the calculated vortex systems to the vortex state in type-II superconductors. The pinning potential is introduced to yield a stable vortex in Sec. IV, where the strength and width of the potential are critically examined for the vortex stabilization. We devote Sec. V to a discussion and conclusion.

II. FORMULATION AND NUMERICAL PROCEDURE

A. Mean-field approximation

We start with the following Hamiltonian, in which Bose particles interact with a two-body potential:

$$\hat{H} = \int d\mathbf{r}\, \hat{\Psi}^\dagger(\mathbf{r}) \left(-\frac{\hbar^2 \nabla^2}{2m} + V(\mathbf{r}) - \mu \right) \hat{\Psi}(\mathbf{r})$$
$$+ \frac{g}{2} \int d\mathbf{r}\, \hat{\Psi}^\dagger(\mathbf{r})\hat{\Psi}^\dagger(\mathbf{r})\hat{\Psi}(\mathbf{r})\hat{\Psi}(\mathbf{r}), \tag{1}$$

where the chemical potential μ is introduced to fix the particle number and $V(\mathbf{r})$ is the confining potential. The two-body interaction between an atom at $\mathbf{r}_1$ and one at $\mathbf{r}_2$ is assumed to be $g\delta(\mathbf{r}_1 - \mathbf{r}_2)$, with g being a positive (repulsive) constant proportional to the s-wave scattering length a, namely, $g = 4\pi\hbar^2 a/m$ (m is the particle mass).

In order to describe the Bose condensation, we assume that the field operator $\hat{\Psi}$ is decomposed into

$$\hat{\Psi}(\mathbf{r}) = \phi(\mathbf{r}) + \hat{\psi}(\mathbf{r}), \tag{2}$$

where the ground-state average is given by

$$\langle \hat{\Psi}(\mathbf{r}) \rangle = \phi(\mathbf{r}). \tag{3}$$

The c number $\phi(\mathbf{r})$ corresponds to the condensate wave function and $\hat{\psi}(\mathbf{r})$ is a q number describing the noncondensate. Substituting the above decomposition (2) in Eq. (1), we obtain

$$\hat{H} = \int d\mathbf{r}\left[\phi^*(\mathbf{r})\left\{ h(\mathbf{r})\phi(\mathbf{r}) + \frac{1}{2}g|\phi(\mathbf{r})|^2 \right\}\phi(\mathbf{r}) \right.$$
$$+ \hat{\psi}^\dagger(\mathbf{r})\{ h(\mathbf{r}) + g|\phi(\mathbf{r})|^2 \}\phi(\mathbf{r}) + \text{H.c.}$$
$$+ \hat{\psi}^\dagger(\mathbf{r})\{ h(\mathbf{r}) + 2g|\phi(\mathbf{r})|^2 \}\hat{\psi}(\mathbf{r})$$
$$+ \frac{g}{2}\hat{\psi}^\dagger(\mathbf{r})\hat{\psi}^\dagger(\mathbf{r})\phi(\mathbf{r})\phi(\mathbf{r}) + \frac{g}{2}\hat{\psi}(\mathbf{r})\hat{\psi}(\mathbf{r})\phi^*(\mathbf{r})\phi^*(\mathbf{r})$$
$$+ g\hat{\psi}^\dagger(\mathbf{r})\hat{\psi}(\mathbf{r})\hat{\psi}(\mathbf{r})\phi^*(\mathbf{r}) + g\hat{\psi}^\dagger(\mathbf{r})\hat{\psi}^\dagger(\mathbf{r})\hat{\psi}(\mathbf{r})\phi(\mathbf{r})$$
$$\left. + \frac{g}{2}\hat{\psi}^\dagger(\mathbf{r})\hat{\psi}^\dagger(\mathbf{r})\hat{\psi}(\mathbf{r})\hat{\psi}(\mathbf{r}) \right], \tag{4}$$

where $h(\mathbf{r}) \equiv -\hbar^2\nabla^2/2m + V(\mathbf{r}) - \mu$ is the one-body Hamiltonian. Let us introduce the variational parameter: The noncondensate density $\rho(\mathbf{r}) = \langle \hat{\psi}^\dagger\hat{\psi} \rangle$ and is approximated as $\hat{\psi}^\dagger\hat{\psi}\hat{\psi} \sim 2\hat{\psi}\rho$ and $\hat{\psi}^\dagger\hat{\psi}^\dagger\hat{\psi}\hat{\psi} \sim 4\hat{\psi}^\dagger\hat{\psi}\rho$.

Then $\hat{H}$ is rewritten as

$$\hat{H} = \int d\mathbf{r}\left[\phi^*(\mathbf{r})\left\{ h(\mathbf{r})\phi(\mathbf{r}) + \frac{1}{2}g|\phi(\mathbf{r})|^2 \right\}\phi(\mathbf{r}) \right.$$
$$+ \hat{\psi}^\dagger(\mathbf{r})\{ h(\mathbf{r}) + g|\phi(\mathbf{r})|^2 + 2g\rho(\mathbf{r}) \}\phi(\mathbf{r}) + \text{H.c.}$$
$$+ \hat{\psi}^\dagger(\mathbf{r})\{ h(\mathbf{r}) + 2g[|\phi(\mathbf{r})|^2 + \rho(\mathbf{r})] \}\hat{\psi}(\mathbf{r})$$
$$\left. + \frac{g}{2}\hat{\psi}^\dagger(\mathbf{r})\hat{\psi}^\dagger(\mathbf{r})\phi(\mathbf{r})\phi(\mathbf{r}) + \text{H.c.} \right]. \tag{5}$$

In order to diagonalize this Hamiltonian, the Bogoliubov transformation is employed, namely, $\hat{\psi}(\mathbf{r})$ is written in terms of the creation and annihilation operators η_q and $\eta_q^\dagger$ and the noncondensate wave functions $u_q(\mathbf{r})$ and $v_q(\mathbf{r})$ as

$$\hat{\psi}(\mathbf{r}) = \sum_q [u_q(\mathbf{r})\eta_q - v_q^*(\mathbf{r})\eta_q^\dagger], \tag{6}$$

where q denotes a set of the quantum numbers. This leads to the diagonalized form $\hat{H} = E_0 + \Sigma_q \varepsilon_q \eta_q^\dagger \eta_q$. The condition that the first-order term in $\hat{\psi}(\mathbf{r})$ vanish yields

$$[h(\mathbf{r}) + g|\phi(\mathbf{r})|^2 + 2g\rho(\mathbf{r})]\phi(\mathbf{r}) = 0. \tag{7}$$

When $\rho(\mathbf{r})$ is made zero, it reduces to the commonly used Gross-Pitaevskii equation

$$[h(\mathbf{r}) + g|\phi(\mathbf{r})|^2]\phi(\mathbf{r}) = 0, \tag{8}$$

which is a nonlinear Schrödinger type equation.

The condition that the Hamiltonian be diagonalized gives rise to the following set of eigenvalue equations for $u_q(\mathbf{r})$ and $v_q(\mathbf{r})$ with the eigenvalue ε_q:

$$[h(\mathbf{r}) + 2g\{|\phi(\mathbf{r})|^2 + \rho(\mathbf{r})\}]u_q(\mathbf{r}) - g\phi^2(\mathbf{r})v_q(\mathbf{r}) = \varepsilon_q u_q(\mathbf{r}), \tag{9}$$

$$[h(\mathbf{r}) + 2g\{|\phi(\mathbf{r})|^2 + \rho(\mathbf{r})\}]v_q(\mathbf{r}) - g\phi^{*2}(\mathbf{r})u_q(\mathbf{r})$$
$$= -\varepsilon_q v_q(\mathbf{r}). \tag{10}$$

The chemical potential μ is contained in h on the left-hand side of Eqs. (9) and (10). Therefore, μ corresponds to the origin of the energy for each eigenvalue ε_q.

The eigenfunctions $u_q(\mathbf{r})$ and $v_q(\mathbf{r})$ must satisfy the normalization condition

$$\int [u_p^*(\mathbf{r})u_q(\mathbf{r})-v_p^*(\mathbf{r})v_q(\mathbf{r})]d\mathbf{r}=\delta_{p,q}. \quad (11)$$

This also means that $\int|u_q|^2 d\mathbf{r}$ is larger than $\int|v_q|^2 d\mathbf{r}$ for an arbitrary q. The variational parameter $\rho(\mathbf{r})$ is determined self-consistently by

$$\rho(\mathbf{r})=\langle\hat{\psi}^\dagger\hat{\psi}\rangle=\sum_q [|u_q(\mathbf{r})|^2 f(\varepsilon_q)+|v_q(\mathbf{r})|^2\{f(\varepsilon_q)+1\}], \quad (12)$$

where $f(\varepsilon)$ is the Bose distribution function. Equations (7) and (9)–(12) constitute a complete set of the self-consistent equations for the PA. The iterative calculations of these equations yield a convergent self-consistent solution.

If the noncondensate component $\rho(r)$ is neglected in this set of equations, the resulting set of the equations yields the so-called Bogoliubov approximation. This was extensively discussed analytically by Pitaevskii [14], Iordanskii [15], and Fetter [16].

The expectation value of the particle number density is given as

$$\langle\hat{n}(\mathbf{r})\rangle=|\phi(\mathbf{r})|^2+\rho(\mathbf{r}), \quad (13)$$

that is, the total density consists of the condensate part $\phi(\mathbf{r})$ and the noncondensate part $\rho(\mathbf{r})$. The particle current density is calculated as

$$\mathbf{j}(\mathbf{r})=\frac{\hbar}{2mi}\{\phi^*(\mathbf{r})\boldsymbol{\nabla}\phi(\mathbf{r})-\phi(\mathbf{r})\boldsymbol{\nabla}\phi^*(\mathbf{r})\}$$
$$+\frac{\hbar}{2mi}\langle\hat{\psi}^\dagger(\mathbf{r})\cdot\boldsymbol{\nabla}\hat{\psi}(\mathbf{r})-\boldsymbol{\nabla}\hat{\psi}^\dagger(\mathbf{r})\cdot\hat{\psi}(\mathbf{r})\rangle. \quad (14)$$

The local density of states is calculated as

$$N(E,r)=\sum_{\mathbf{q}} \{|u_{\mathbf{q}}(r)|^2+|v_{\mathbf{q}}(r)|^2\}\delta(\varepsilon_{\mathbf{q}}-E). \quad (15)$$

This quantity was observed directly by scanning tunneling microscopy for a vortex in superconductors [30].

B. Vortex description

We now consider a cylindrically symmetric system that is characterized by the radius R and the height L. We use the cylindrical coordinate $\mathbf{r}=(r,\theta,z)$. We impose the boundary conditions that all the wave functions vanish at the wall $r=R$, which is taken far enough from the vortex center at $r=0$ and the periodic boundary condition along the z axis. When a vortex line passes through the center of the cylinder, the condensate wave function $\phi(\mathbf{r})$ is expressed as

$$\phi(r,\theta,z)=\phi(r)e^{iw\theta}, \quad (16)$$

where $\phi(r)$ is a real function and w is the winding number. $w=0$ corresponds to the non-vortex case and $w=1$ to the vortex case. The $w\geqslant 2$ case is not considered here because this state is energetically too unstable. The noncondensate density $\rho(\mathbf{r})$ is a real function, depending only on r, that is, $\rho(r,\theta,z)=\rho(r)$. It is also seen from Eqs. (9) and (10) that the phases of $u_q(\mathbf{r})$ and $v_q(\mathbf{r})$ are written as

$$u_{\mathbf{q}}(\mathbf{r})=u_q(r)e^{iq_z z}e^{i(q_\theta+w)\theta}, \quad (17)$$

$$v_{\mathbf{q}}(\mathbf{r})=v_q(r)e^{iq_z z}e^{i(q_\theta-w)\theta}. \quad (18)$$

The set of the quantum numbers $\mathbf{q}$ in Eq. (6) is described by (q_r,q_θ,q_z), where $q_r=1,2,3,\ldots,q_\theta=0,\pm 1,\pm 2,\ldots$, and $q_z=0,\pm 2\pi/L,\pm 4\pi/L,\ldots$. Note that only $u(r)(q_\theta=-1)$ and $v(r)(q_\theta=1)$ are nonvanishing at $r=0$.

By following the method by Gygi and Schlüter [31], the functions $u_q(r)$ and $v_q(r)$ are expanded in terms of

$$\varphi_\nu^{(i)}(r)\equiv\frac{\sqrt{2}}{J_{|\nu|+1}(\alpha_{|\nu|}^{(i)})}J_{|\nu|}\left(\alpha_{|\nu|}^{(i)}\frac{r}{R}\right) \quad (19)$$

as

$$u_q(r)=\sum_i c_q^{(i)}\varphi_{q_\theta+w}^{(i)}(r), \quad (20)$$

$$v_q(r)=\sum_i d_q^{(i)}\varphi_{q_\theta-w}^{(i)}(r), \quad (21)$$

where $J_\nu(r)$ is the Bessel function of νth order and $\alpha_\nu^{(i)}$ denotes ith zero of J_ν. The eigenvalue problem of Eqs. (9) and (10) are reduced to diagonalizing the matrix

$$\begin{pmatrix} A_{i,j}(q_\theta+w,q_z) & -B_{i,j}(q_\theta,w) \\ B_{i,j}^{\mathrm{T}}(q_\theta,w) & -A_{i,j}(q_\theta-w,q_z) \end{pmatrix}\begin{pmatrix} c_{\mathbf{q}}^{(1)} \\ c_{\mathbf{q}}^{(2)} \\ \vdots \\ d_{\mathbf{q}}^{(1)} \\ d_{\mathbf{q}}^{(2)} \\ \vdots \end{pmatrix}$$

$$=\varepsilon_{\mathbf{q}}\begin{pmatrix} c_{\mathbf{q}}^{(1)} \\ c_{\mathbf{q}}^{(2)} \\ \vdots \\ d_{\mathbf{q}}^{(1)} \\ d_{\mathbf{q}}^{(2)} \\ \vdots \end{pmatrix} \quad (22)$$

for each q_θ and q_z, where

$$A_{i,j}(\nu,q_z)=\frac{\hbar^2}{2m}\left\{\left(\frac{\alpha_\nu^{(j)}}{R}\right)^2+q_z^2\right\}\delta_{i,j}-\mu\delta_{i,j}$$
$$+\int_0^R [V+2g(\phi^2+\rho)]\varphi_\nu^{(i)}\varphi_\nu^{(j)}r\,dr, \quad (23)$$

$$B_{i,j}(q_\theta, w) = \int_0^R g\,\phi^2\,\varphi^{(i)}_{q_\theta+w}\varphi^{(j)}_{q_\theta-w}\,r\,dr. \qquad (24)$$

The following symmetry relation should be noted:

$$(c,d,\varepsilon) \text{ for } q_\theta \Leftrightarrow (d,c,-\varepsilon) \text{ for } -q_\theta. \qquad (25)$$

We determined the signs of q_θ and ε by the normalization condition (11).

It is not self-evident *a priori* that Eq. (22) gives real eigenvalues because the Hamiltonian matrix in Eq. (22) is not symmetric. However, these eigenvalues can be proved to be real (positive or negative) in a way similar to that of Fetter [16]. The circulating current density $j_\theta(r)$ in Eq. (14) is expressed as

$$j_\theta(r) = j^{(1)}_\theta(r) + j^{(2)}_\theta(r), \qquad (26)$$

$$j^{(1)}_\theta(r) = \frac{\hbar}{m}\frac{w}{r}\phi^2(r), \qquad (27)$$

$$j^{(2)}_\theta(r) = \frac{\hbar}{m}\sum_{\mathbf{q}}\left\{\frac{q_\theta+w}{r}|u_{\mathbf{q}}(r)|^2 f(\varepsilon_{\mathbf{q}})\right.$$
$$\left. -\frac{q_\theta-w}{r}|v_{\mathbf{q}}(r)|^2[f(\varepsilon_{\mathbf{q}})+1]\right\}, \qquad (28)$$

where the total current consists of the condensate component $j^{(1)}_\theta(r)$ and the noncondensate $j^{(2)}_\theta(r)$.

C. Calculated system

We have performed self-consistent calculations of a gas of Na atoms trapped radially by a harmonic potential $V(r) = \frac{1}{2}m(2\pi\nu_r)^2 r^2$. We use the following parameters: $m = 3.81\times10^{-26}$ kg, the scattering strength $a = 2.75$ nm, and the radial trapping frequency $\nu_r = 200$ Hz. The area density per unit length along the z axis is chosen to be $n_z = 2 \times 10^4$ μm^{-1}, so that the peak density will be $O(10^{20}$ m$^{-3})$. The system size is set to $R = 20$ μm and $L = 10$ μm.

We have employed the energy cutoff method to calculate Eqs. (12) and (28) where the calculation terminates when the obtained eigenvalues exceeds about $80\hbar\nu_r$. This method treats $\sim 80\,000$ eigenfunctions, although it is its lowest two modes, namely, the condensate state and the lowest core localized state (LCLS), that play a significant role.

III. STABLE QUANTIZED VORTEX AT FINITE TEMPERATURES

The isolated single quantized vortex is unstable within certain mean-field approximations [19,21] in a nonrotating system. When the lowest excitation eigenvalue of the system becomes lower than the energy of the condensate, the whole calculation based on the assumption that the energy for the condensate is lowest [19] is invalidated. This means that the vortex is unstable.

In the finite-T calculations shown below the quantized vortex becomes stable in the BEC systems confined by a harmonic potential above a certain temperature. We analyze
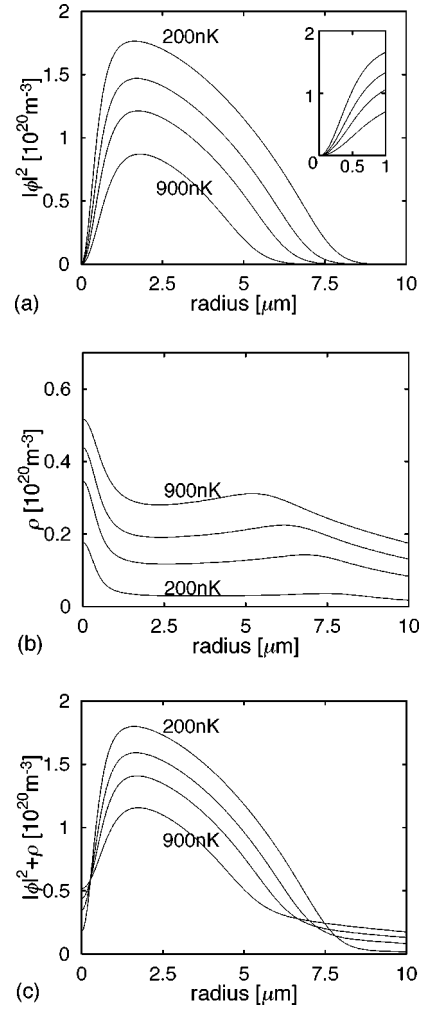

FIG. 1. (a) Condensate density $|\phi(r)|^2$ at various T. The total particle number of the condensate $|\phi(r)|^2$ decreases as T increases. The inset shows the profile of $|\phi(r)|^2$ at small r. (b) Noncondensate density $\rho(r)$, which increases with increasing T. The characteristic length scale near the center corresponds to the core radius of $|\phi|^2$ in (a). (c) Total density $|\phi(r)|^2 + \rho(r)$. Each figure shows the densities at $T = 200$, 500, 700, and 900 nK.

how the vortex state at finite T can become stabilized and examine fundamental properties of a stable vortex.

A. Spatial structures of a condensate and a noncondensate

The spatial profiles of the condensate and noncondensate densities for several temperatures are shown in Figs. 1(a) and 1(b), respectively. It is seen from Fig. 1(a) that the condensate $|\phi(r)|^2$ vanishes and changes quadratically (proportional to r^2) near the vortex center $r = 0$, which is in contrast to the linear behavior (proportional to r) in the Gross-Pitaevskii theory (8). This unique shape of $|\phi(r)|^2$ reflects the rounded shape of the $2g\rho(\mathbf{r})$ term in Eq. (7). [This $\rho(\mathbf{r})$ is depicted in Fig. 1(b).]

This feature differs also from the superconducting case where the pair potential changes linearly [28]. As T increases, the core radius increases, as seen from the inset. The condensate is pushed outward and converted into the noncondensate. Thus the total particle number of the condensate
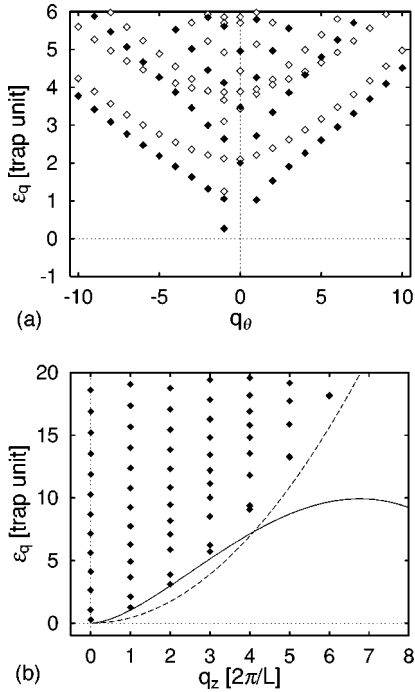
FIG. 2. Dispersion relations of the eigenvalues $\varepsilon_{\mathbf{q}}$ at $T = 200$ nK. (a) Along q_θ. The solid diamonds are states with $q_z = 0$. The lowest solid diamond at each q_θ corresponds to $q_r = 1$, the second lowest to $q_r = 2$, and so on. (b) Eigenvalues along q_z. Only the $q_\theta = -1$ states are plotted. The solid curve is explained in the text below Eq. (30). The dashed curve denotes $(\hbar^2/2m)q_z^2$.

decreases monotonically as T increases.

In Fig. 1(b) the spatial variation of the noncondensate density $\rho(r)$ is displayed. Reflecting the core structure, the noncondensate fraction accumulates at the vortex center. The core radius grows as T increases, as seen from Fig. 1(b), which will be analyzed in more detail shortly.

The overall feature of the spatial change of the total density consisting of the condensate and noncondensate $|\phi(r)|^2 + \rho(r)$ is shown in Fig. 1(c). As T increases, the spatial profile tends to distribute uniformly and the maximum position of the density from the core also increases, indicating that the effective core radius expands. The total density does not vanish anywhere inside the confined potential even at the vortex core. It is also interesting to notice the existence of a focal point near the center that does not move as T changes.

B. Excitation spectra

In Figs. 2(a) and 2(b) we display the dispersion relations of the eigenvalues along q_θ and q_z, respectively. The excitation modes are not symmetric about the q_θ axis because of the presence of the circulation. However, at the higher energies the distribution of these eigenmodes become symmetric. The modes characterized by $q_z = 0$ are shown as solid diamonds in Fig. 2(a). The lowest eigenmode at $q_\theta = -1$ is very important in the understanding of the mechanism of vortex stabilization.

The modes with $(q_r, q_\theta) = (1, -1)$ and various q_z including the LCLS correspond to the so-called Kelvin mode known in classical vortex. In Fig. 2(b) we display the dispersion relations of the eigenvalues with $q_\theta = -1$ along q_z.
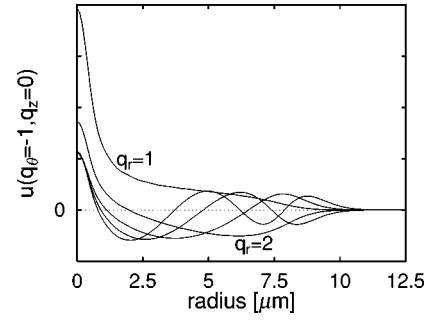
FIG. 3. Wave functions $u(r)$ ($q_\theta = -1$ and $q_z = 0$) at $T = 200$ nK. The radial quantum number q_r varies from 1 to 5. Each $u(r)$ has node(s) whose number is equal to q_r. These states are localized at the core. The vertical axis is in arbitrary units.

This dispersion relation is predicted by Pitaevskii [14] in a spatially uniform system with density n_{uni}, except near the core within the BA, at the long-wavelength limit as

$$\varepsilon(q_r = 1, q_\theta = -1, q_z) = \frac{\hbar^2 q_z^2}{2m} \ln \frac{1}{q_z \xi_{\text{uni}}} \quad (q_z \xi_{\text{uni}} \ll 1),$$
$$(29)$$

which is called the Kelvin mode, where

$$\xi_{\text{uni}} \equiv \frac{\hbar}{\sqrt{2mn_{\text{uni}}g}}.$$
$$(30)$$

The dispersion relation of the corresponding modes with $q_\theta = -1$ is shown in Fig. 2(b) as the lowest edge. We have tried to fit this prediction (29) with our result by substituting various n_{uni} in ξ_{uni} of Eq. (30). The solid curve in Fig. 2(b) shows $n_{\text{uni}} = 0.1 n_{\text{peak}}$. The fitting is rather satisfactory.

The spatial profiles of the eigenfunctions with $q_\theta = -1$ are depicted in Fig. 3. There is no rapid spatial oscillation in these eigenfunctions corresponding to the Friedel oscillation seen in the Fermi systems [31,32]. It is also noticed that a slow oscillation of the condensate near the vortex core seen in several Monte Carlo computations [33] for superfluid ^{4}He is absent here. The present weakly interacting case differs from that in the strongly interacting system in several respects.

C. Vortex stabilization at finite T

We discuss the origin of vortex stabilization. Let us start with the particle number densities $|\phi(r)|^2$ (condensate) and $\rho(r)$ (noncondensate) in Fig. 1. It is the eigenstates that compose the whole system. The wave function $\phi(r)$ with the energy μ corresponds to the condensate fraction and the noncondensate density $\rho(r)$ is composed of the eigenstates with the eigenvalues and the wave functions $\varepsilon_{\mathbf{q}}, u_{\mathbf{q}}(r)$, and $v_{\mathbf{q}}(r)$. The eigenstate with $\varepsilon_{\mathbf{q}} = 0$ that equals μ corresponds to the condensate.

The states with the angular momentum index $q_\theta = -1$, whose relative motion to the circulating current of the condensate is at rest in the laboratory frame [$q_\theta + w$ in Eq. (17) is equal to zero], are likely to have the lowest eigenvalue among various states. It is the eigenstate $\mathbf{q} \equiv (q_r, q_\theta, q_z) = (1, -1, 0)$ whose eigenvalue becomes negative and leads to
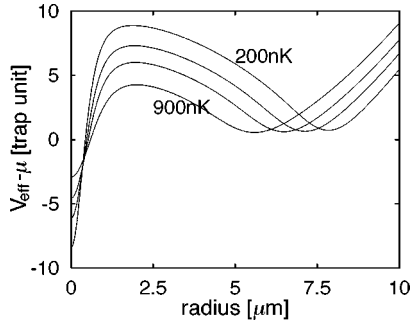
FIG. 4. Effective potential $V_{\mathrm{eff}}(r)$ at temperatures $T = 200$, 500, 700, and 900 nK. We subtract the chemical potential μ from $V_{\mathrm{eff}}(r)$ at each T.

the vortex instability. The spatial profiles of the eigenfunctions $\mathbf{q} = (1-5, -1, 0)$ are depicted in Fig. 3. We can see that these states are localized near the core ($r = 0$). Solid diamonds at $q_\theta = -1$ in Fig. 2(a) correspond to the wave functions in Fig. 3. We can see that the lowest mode $\mathbf{q} = (-1, 0, 1)$ is strongly localized at $r = 0$. Let us call this state the lowest core localized state. The vortex state is (meta)stable as long as the LCLS exists with a positive eigenvalue. Now the question is why the energy of the LCLS is positive at finite T, as shown in Fig. 2(a).

We define the effective potential

$$V_{\mathrm{eff}}(r) \equiv V(r) + 2g[\,|\phi(r)|^2 + \rho(r)], \qquad (31)$$

whose combination appears in the eigenvalue equations (9) and (10). The eigenvalues of various modes are estimated by integrating $V_{\mathrm{eff}}(r)$ with each of the wave functions over the spatial volume. Of course the LCLS is not an exception. The shape of $V_{\mathrm{eff}}(r)$ near the core ($r \sim 0$) determines the eigenvalues of the LCLS. As seen from Fig. 4, $V_{\mathrm{eff}}(r)$ at the vortex center is pushed upward as T increases. This is why the LCLS has a positive eigenvalue. Although the vortex stability seems to increases with T, the determination of the stability conditions is a complex problem and is discussed in Sec. III D. The increase of $V_{\mathrm{eff}}(r)$ near the core is caused by the contribution from the noncondensate $\rho(r)$. Thus $V_{\mathrm{eff}}(r)$, and especially the term $2g\rho(r)$ in Eq. (31), works as an effective pinning potential that prevents the vortex from moving outward. Now let us consider why the noncondensate $\rho(r)$ has a peak at the core.

The noncondensate density $\rho(r)$ is composed of the wave functions $u(r)$ and $v(r)$, as seen in Eq. (12). Note that only $u(r)$ ($q_\theta = -1$) and $v(r)$ ($q_\theta = 1$) are nonvanishing at $r = 0$, as mentioned before. The localization of $\rho(r)$ at small r mainly comes from the LCLS term $[\mathbf{q} = (1, -1, 0)]$ in Eq. (12). Figure 3 again shows that the $|u(r)|^2$ coefficient of this term is strongly localized at $r = 0$ and Fig. 2(a) shows that the $f(\varepsilon)$ coefficient has a huge value because the eigenvalue ε is very small. Note that $f(\varepsilon)$ is the Bose distribution function and $\lim_{\varepsilon \to 0} f(\varepsilon) = +\infty$. The LCLS, whose eigenvalue is approaching zero from above, itself forms a pinning potential to keep the eigenvalue positive combined with the Bose distribution function. We can see the wave functions and the eigenvalues in Fig. 7, which displays the local density of states defined by Eq. (15). This may be helpful to understand the dominance of the LCLS in $\rho(r)$ at small r.
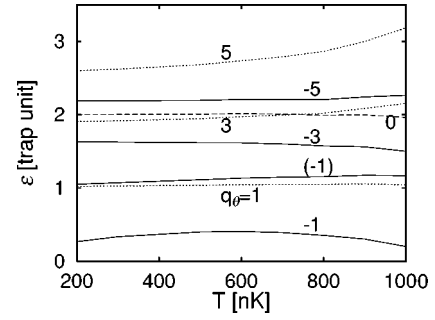

FIG. 5. Eigenvalues ε of the selected lowest modes as a function of T. The number of each line denotes q_θ. All of the lines are eigenvalues with $q_r = 1$ and $q_z = 0$, except the line labeled (-1), with $\mathbf{q} = (2, -1, 0)$. Solid lines, $q_\theta < 0$; dotted lines, $q_\theta > 0$; dashed line, $q_\theta = 0$. While the dipole mode with $q_\theta = 1$ is exceptionally almost T independent and fixed to $\varepsilon = 1$, coinciding with the trapped frequency, other modes with $q_\theta > 0$ ($q_\theta \leqslant 0$) tend to increase (decrease) with increasing T. The eigenvalues with large q_θ, which are not shown here, generally increase. This is because these wave functions generally lie at a large radius and the effective potential $V_{\mathrm{eff}}(r)$ there increases with increasing T. See the large radius side of Fig. 4.

This mechanism of the T-dependent stabilization is based on the PA. It introduces the noncondensate density $\rho(r)$ as an effective potential ignoring the anomalous average $\langle \psi\psi \rangle$, which describes the interaction effects between the condensate and the noncondensate. An improvement of the PA towards this direction has been attempted by Hutchinson et al. [23].

It is also obvious that large enough $V_{\mathrm{eff}}(r)$ near the center is decisive in stabilizing the vortex, irrespective of the origin coming from either $g\rho(r)$ or $V(r)$. The deformation of $V(r)$ also stabilizes the vortex state. This stabilization mechanism depends neither on the PA nor on the interaction between $\rho(r)$ and $\phi(r)$. This deformation of $V(r)$ is discussed in Sec. IV and the rest of this section is devoted to the various properties of the T-stabilized system that has been obtained.

D. Stability

As mentioned before, the determination of the stability conditions is a complex problem. It is natural to consider the eigenvalue $\varepsilon > 0$ for the LCLS and large enough $V_{\mathrm{eff}}(r)$ at $r = 0$ as possible conditions for the stability. What makes the matter complicated is the relation of these two conditions. Expressed more explicitly,

$$V_{\mathrm{eff}}(0) = g|u_{\mathrm{LCLS}}(0)|^2 f(\varepsilon_{\mathrm{LCLS}})$$

$$+ [\text{other contributions from}$$

$$u(q_\theta = -1)\text{'s and } v(q_\theta = 1)\text{'s}]. \qquad (32)$$

The T dependence of the selected lowest modes are displayed in Fig. 5. As anticipated from the T dependence of the lowest mode, which gradually decreases on lowering T, the whole calculation breaks down when this mode becomes negative from above. However, this lowering process of ε with T will not proceed smoothly because the Bose distribu-
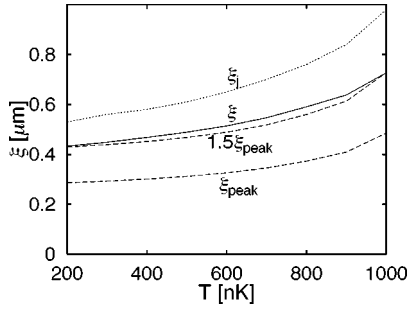
FIG. 6. T dependences of ξ's for various definitions. Both ξ (solid line) and ξ_{peak} (lower dashed line) are defined in the text. The upper dashed line denotes $1.5\xi_{peak}$. The dotted line labeled ξ_j is the peak radius of $j_\theta(r)$.

tion function at small ε could make the pinning part of $V_{eff}(r)$ very large. When $T=0$, the effective potential at the center

$$V_{eff}(0) = g \sum_{\mathbf{q}\,(q_\theta=1)} |v_{\mathbf{q}}(0)|^2 \qquad (33)$$

is not likely to become large enough, although we cannot exclude its possibility completely.

We only point out that these problems are open and shall not discuss them further in this paper. We failed to determine the self-consistent density profiles $\rho(r)$ and $|\phi(r)|^2$ for $T < 200$ nK, which is the lowest temperature we can reach.

E. Core radius

Figures 1(a)–1(c) show that the core radius increases as T increases. We define here the core radius by the distance ξ from the center where $\frac{1}{2}\max[|\phi(r)|^2]=|\phi(\xi)|^2$. The T dependence of this ξ is exhibited in Fig. 6. The core radius $\xi(T)$ is seen to be T-dependent and decrease as T is lowered. We define $\xi_{peak}\equiv\hbar/\sqrt{2mn_{peak}g}$, where $n_{peak}\equiv\max[|\phi(r)|^2]$ is the peak density of the condensate. This resembles the classical definition [16] of the coherence length ξ_{uni} in Eq. (30) for a uniform system. The core radius ξ is almost equal to $1.5\xi_{peak}$, as seen in Fig. 6.

The total current density $j_\theta^{(1)}(r)+j_\theta^{(2)}(r)$ defined in Eq. (26) is shown in inset of Fig. 8. The distance from the vortex center at which the current amplitude takes a maximum is another measure of the vortex core radius. This quantity ξ_j shown in Fig. 6 also decreases upon lowering T.

F. Local density of states

The local density of states $N(r,E)$ given by Eq. (15) is shown in Fig. 7. The states with $q_\theta=-1$ are seen to localize at the vortex center, giving rise to several prominent peaks in the local density of states.

These features around the core may be observable and should be compared with those in vortices in a superconductor where extensive studies have been compiled [28]. This is particularly true for the localized excitations near a vortex core studied by Caroli *et al.* [36,37]. These core excitations are now recognized to be decisive in the understanding of the fundamental properties of the vortex. The Popov theory corresponds to the so-called Bogoliubov–de
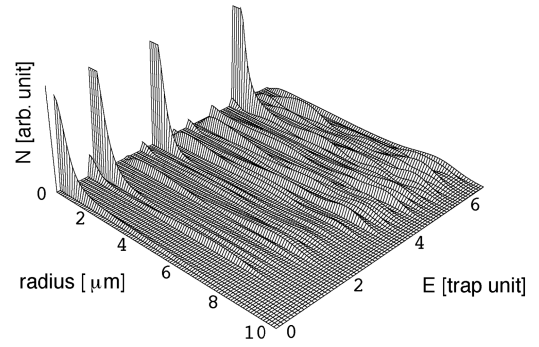

FIG. 7. Local density of states $N(r,E)$ with the lower-energy side ($0<E<7$ in trap units) at $T=200$ nK. The states distinctively localized near the core correspond to the angular momentum $q_\theta=-1$. The sharp peak on the left (low-energy) side is the LCLS. Some too-high peaks around the core are cut at a certain value of $N(r,E)$.

Gennes theory in their mathematical structures, which is widely used to treat various spatially nonuniform superconductors having an interface or a vortex [31,32].

We also note that in superconductors $N(r,E)$ is directly observed using scanning tunneling microscope [30] and analyzed theoretically within the similar theoretical framework [31,32,34] quite successfully. The characteristic core radius is estimated as the coherence length ~ 0.5 μm, which is contrasted with a few angstroms in superfluid ^{4}He. Thus there is a good chance to investigate the detailed core structure of the present BEC systems.

G. Circulating current density

The total current density $j_\theta^{(1)}(r)+j_\theta^{(2)}(r)$ defined in Eq. (26) is shown in inset of Fig. 8. The noncondensate contribution $j_\theta^{(2)}(r)$ and its q_θ components are depicted in the main panel of Fig. 8. In the immediate vicinity of the core $j_\theta^{(2)}(r)$ is governed by the $q_\theta=0$ and the $q_\theta=-2$ components. The positive (negative) q_θ's give rise to the positive (negative) contribution to $j_\theta(r)$, except for the $q_\theta=-1$, which has positive contribution. The $|u(r)|^2$ term is dominant in most q_θ of Eq. (28). This is why positive (negative) q_θ's give the positive (negative) contribution. Since we are treating systems with $w=1$, the $(q_\theta+w)/r$ coefficients of the $|u(r)|^2$ terms become zero and the $|v(r)|^2$ terms with positive sign become relevant when $q_\theta=-1$. This is why the
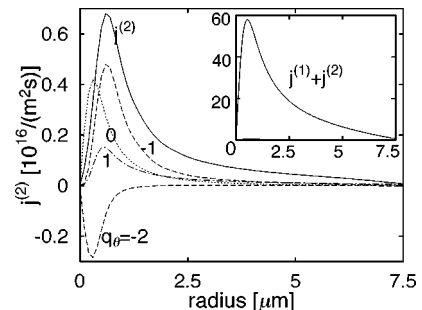

FIG. 8. Noncondensate contribution $j_\theta^{(2)}(r)$ of the particle current density at $T=200$ nK. Each component with $q_\theta=0,\pm1,-2$ is shown separately. The inset shows the total current density $j_\theta(r)$ $\equiv j_\theta^{(1)}(r)+j_\theta^{(2)}(r)$.
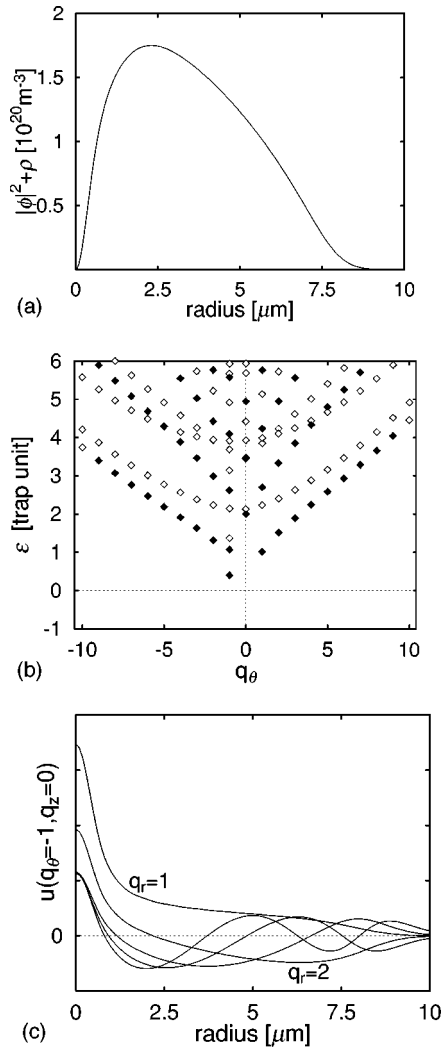
FIG. 9. Various properties of a vortex system stabilized by the pinning potential in Eq. (34). $V_0 = 5$ (trap units), $r_0 = 1$ μm, and $T = 0$ K. (a) Total particle number density. (b) Dispersion relations of the eigenvalues ε along q_θ. Solid diamonds are eigenvalues with $q_z = 0$. (c) Wave functions $u(r)$ ($q_r = 1$–5, $q_\theta = -1$, and $q_z = 0$). The vertical axis is in arbitrary units.

FIG. 10. Various properties of a vortex system stabilized by the pinning potential. $V_0 = 50$ (trap units), $r_0 = 1$ μm, and $T = 0$ K. (a) Total particle number density. (b) Dispersion relations of the eigenvalues ε along q_θ. Solid diamonds are eigenvalues of $q_z = 0$. (c) Wave functions $u(r)$ ($q_r = 1$–5, $q_\theta = -1$, and $q_z = 0$). The vertical axis is in arbitrary units.

$q_\theta = -1$ component gives a positive, not negative, contribution. The net result gives a finite contribution to superfluid flow from the noncondensate.

IV. VORTEX STABILIZATION BY THE PINNING POTENTIAL AT $T = 0$

It is now clear that the introduction of a pinning potential at the vortex center stabilizes the quantized vortex even at $T = 0$. Here we explicitly demonstrate it by a model pinning potential described by

$$V_{\text{pinning}}(r) = V_0 e^{-r^2/2r_0^2} \qquad (34)$$

in addition to the harmonic potential. This pinning potential may be realized by focusing a laser beam on the vortex center. Since we are imposing the periodic boundary condition along the z axis, topologically the system is equivalent to a toroidal geometry if the system length L is large enough.
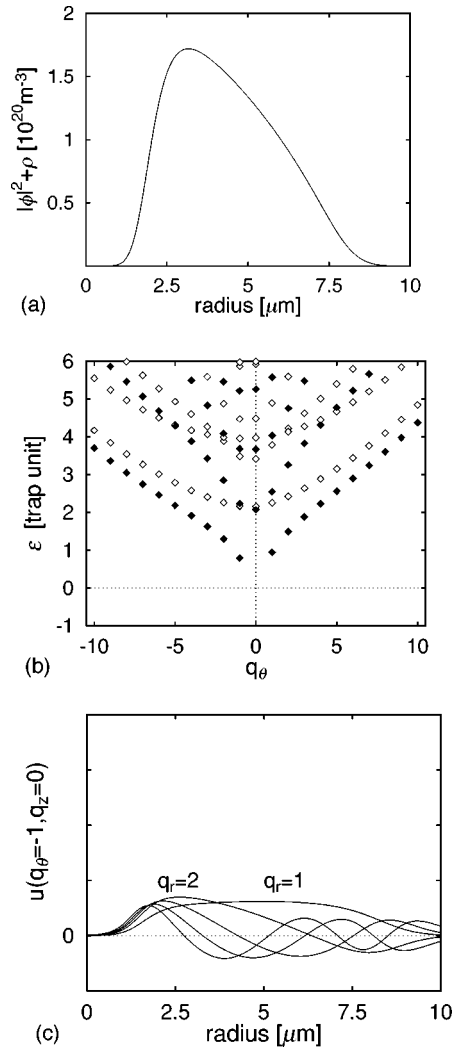
We have done self-consistent calculations at $T = 0$ in the presence of the pinning potential using the same method as in Sec. III. The self-consistent solution for the $V_0 = 5$ trap units and $r_0 = 1$ μm and the other parameters, which are the same as before, is depicted in Figs. 9(a)–9(c). It is seen from these figures that the vortex is stable because the LCLS is now all positive, as shown in Fig. 9(b), allowing the fully self-consistent solution. We note that the eigenfunction $u(r)$ ($q_r = 1$) shown in Fig. 9(c) still has a large amplitude at $r = 0$. The condensate is pushed outward because of the pinning potential and its initial rise at the vortex core is steep [Fig. 9(a)]. The noncondensate fraction is vanishingly small in this example at $T = 0$.

In a larger pinning potential ($V_0 = 50$ trap units and $r_0 = 1$ μm) exemplified in Fig. 10 the condensate is pushed farther outward and the vortex center is empty space [Fig. 10(a)]. It resembles a ring-shaped BEC systems that has been considered theoretically [21,35]. The wave functions of the states $\mathbf{q} = (1-5, -1, 0)$ in Fig. 10(b) are squeezed at small r

by the pinning potential. There is no LCLS. This deformation of $u(r)$ directly lifts the eigenvalue of the lowest eigenstate at $q_\theta = -1$ in Fig. 10(b) to stabilize further the vortex state. The overall distribution of the excitation spectrum is almost symmetric about the q_θ axis [Fig. 10(b)]. All the corresponding eigenfunctions with $q_\theta = -1$ vanish at $r=0$ [Fig. 10(c)], which is contrasted with those in Figs. 3 and 9(c).

V. CONCLUSION AND DISCUSSION

We have investigated the stability conditions of a vortex in BEC systems by performing microscopic self-consistent calculations based on the Popov approximation. It is demonstrated that the BEC systems confined in a harmonic potential at finite temperatures sustain the stable vortex. This is contrasted with the cases in the absence of the pinning potential where the same calculation yields an unstable vortex, as shown previously [19,21]. The vortex instability comes from the negative eigenvalue of the lowest core localized state. Therefore, physically it is possible to lift this energy by increasing the effective potential experienced by this quasiparticle. This can be realized by raising T or introducing an external pinning potential. In the former case the LCLS itself acts as the effective pinning potential, amplified through the Bose distribution function. The presence of the noncondensate in the Popov theory enables this T-dependent mechanism.

The detailed vortex properties are analyzed for the stable vortex. Several eminent features are worth mentioning. (i) The condensate $|\phi(r)|^2$ behaves proportionally to r^2 near the vortex core and the noncondensate has a peak at the core. (ii) The characteristic length or the core radius is well described by a formula $\hbar/\sqrt{2mn_{peak}g}$, with n_{peak} being the peak density of the condensate. (iii) The particle density is nonvanishing everywhere inside a system even at the core center when a system is T stabilized. (iv) The local density of states exhibits large peak structures at the core center for the low-energy side and the peaks indicate the existence of the LCLS and other core localized states. These characteristics may be directly observed once the quantized vortex is realized in the present BEC systems.

We hope that the vortex state in BEC of an alkali-metal atom gas should come true experimentally. If realized, we may have a chance to unify theories of the present dilute BEC systems and the strongly interacting superfluid ^{4}He systems. We also hope that the precise and detailed analysis of the vortex core structure should be possible because an advantage here is that the length scale of the core radius is much larger than those in superfluid ^{4}He or superconductors.

[1] M. H. Anderson, J. R. Ensher, M. R. Matthews, C. E. Wieman, C. E. Wieman, and E. A. Cornell, Science **269**, 198 (1995).

[2] C. C. Bradley, C. A. Sackett, J. J. Tollett, and R. G. Hulet, Phys. Rev. Lett. **75**, 1687 (1995).

[3] K. B. Davis, M.-O. Mewes, M. R. Andrews, N. J. van Druten, D. D. Durfee, D. M. Kurn, and W. Ketterle, Phys. Rev. Lett. **75**, 3969 (1995).

[4] *Bose-Einstein Condensation*, edited by A. Griffin, D. W. Snoke, and S. Stringari (Cambridge University Press, Cambridge, 1995).

[5] For a review see F. Dalfovo, S. Giorgini, L. P. Pitaevskii, and S. Stringari, e-print cond-mat/9806038.

[6] S. Inouye, M. R. Andrews, J. Stenger, H.-J. Miesner, D. M. Stamper-Kurn, and W. Ketterle, Nature (London) **392**, 151 (1998).

[7] D. M. Stamper-Kurn, M. R. Andrews, A. P. Chikkatur, S. Inouye, H.-J. Miesner, J. Stenger, and W. Ketterle, Phys. Rev. Lett. **80**, 2027 (1998).

[8] T. Ohmi and K. Machida, J. Phys. Soc. Jpn. **67**, 1822 (1998).

[9] T. L. Ho, e-print cond-mat/9803231.

[10] K.-P. Marzlin and W. Zhang, Phys. Rev. A **57**, 3801 (1998); **57**, 4761 (1998).

[11] B. Jackson, J. F. McCann, and C. S. Adams, Phys. Rev. Lett. **80**, 3903 (1998).

[12] N. Bogoliubov, J. Phys. (Moscow) **11**, 23 (1947).

[13] E. P. Gross, Nuovo Cimento **20**, 454 (1961); J. Math. Phys. **4**, 195 (1963).

[14] L. P. Pitaevskii, Zh. Éksp. Teor. Fiz. **40**, 646 (1961) [Sov. Phys. JETP **13**, 451 (1961)].

[15] S. V. Iordanskii, Zh. Éksp. Teor. Fiz. **49**, 225 (1965) [Sov. Phys. JETP **22**, 160 (1966)].

[16] L. Fetter, Phys. Rev. **138**, A709 (1965); **140**, A452 (1965); Ann. Phys. (N.Y.) **70**, 67 (1972).

[17] V. N. Popov, *Functional Integrals and Collective Excitations* (Cambridge University Press, Cambridge, 1987).

[18] For various applications of mean-field theories to the present finite systems see V. V. Goldman, I. F. Silvera, and A. J. Leggett, Phys. Rev. B **24**, 2870 (1981); D. A. Huse and E. D. Siggia, J. Low Temp. Phys. **46**, 137 (1982); M. Edwards and K. Burnett, Phys. Rev. A **51**, 1382 (1995); P. A. Ruprecht, M. J. Holland, K. Burnett, and M. Edwards, *ibid.* **51**, 4704 (1995).

[19] T. Isoshima and K. Machida, J. Phys. Soc. Jpn. **66**, 3502 (1997).

[20] R. J. Dodd, K. Burnett, M. Edwards, and C. W. Clark, Phys. Rev. A **56**, 587 (1997).

[21] D. S. Rokhsar, Phys. Rev. Lett. **79**, 2164 (1997); e-print cond-mat/9709212.

[22] T. Isoshima and K. Machida, J. Phys. Soc. Jpn. **67**, 1840 (1998).

[23] D. A. W. Hutchinson, R. J. Dodd, and K. Burnett, Phys. Rev. Lett. **81**, 2198 (1998).

[24] M. Edwards, R. J. Dodd, C. W. Clark, P. A. Ruprecht, and K. Burnett, Phys. Rev. A **53**, R1950 (1996); F. Dalfovo and S. Stringari, *ibid.* **53**, 2477 (1996).

[25] S. Sinha, Phys. Rev. A **55**, 4325 (1997). This paper treats semiclassically an equation similar to ours.

[26] A. A. Svidzinsky and A. L. Fetter, e-print cond-mat/9803181.

[27] R. J. Donnelly, *Quantized Vortices in Helium II* (Cambridge University Press, Cambridge, 1991).

[28] For a review, see A. L. Fetter and P. C. Hohenberg, in *Superconductivity*, edited by R. D. Parks (Dekker, New York, 1969).

[29] D. A. W. Hutchinson, E. Zaremba, and A. Griffin, Phys. Rev. Lett. **78**, 1842 (1997).

[30] H. Hess, R. B. Robinson, and J. V. Waszczak, Phys. Rev. Lett. **64**, 2711 (1990).

[31] F. Gygi and M. Schlüter, Phys. Rev. B **43**, 7609 (1991).

[32] N. Hayashi, T. Isoshima, M. Ichioka, and K. Machida, Phys. Rev. Lett. **80**, 2921 (1998).

[33] G. V. Chester, R. Metz, and L. Reatto, Phys. Rev. **175**, 275 (1968); F. Dalfovo, Phys. Rev. B **46**, 5482 (1992).

[34] N. Hayashi, M. Ichioka, and K. Machida, Phys. Rev. Lett. **77**, 4074 (1996); Phys. Rev. B **56**, 9052 (1997).

[35] E. J. Mueller, P. M. Goldbart, and Y. L. Geller, Phys. Rev. A **57**, R1505 (1998).

[36] C. Caroli, P. G. de Gennes, and J. Matricon, Phys. Lett. **9**, 307 (1964); C. Caroli and J. Matricon, Phys. Kondens. Mater. **3**, 380 (1965).

[37] J. Bardeen, R. Kümmel, A. E. Jacobs, and L. Tewordt, Phys. Rev. **187**, 556 (1969).